JCTC Journal of Chemical Theory and Computation

Article

Cite This: J. Chem. Theory Comput. 2019, 15, 3260−3271

pubs.acs.org/JCTC

A Transferable, Multi-Resolution Coarse-Grained Model for Amorphous Silica Nanoparticles

Andrew Z. Summers,[†,‡] Christopher R. Iacovella,[†,‡] Olivia M. Cane,[†,‡] Peter T. Cummings,[†,‡] and Clare McCabe*[,†,‡,§]

[†]Department of Chemical and Biomolecular Engineering, [‡]Multiscale Modeling and Simulation (MuMS) Center, and [§]Department of Chemistry, Vanderbilt University, Nashville, Tennessee 37235, United States

Supporting Information

ABSTRACT: Despite the ubiquity of nanoparticles in modern materials research, computational scientists are often forced to choose between simulations featuring detailed models of only a few nanoparticles or simplified models with many nanoparticles. Herein, we present a coarse-grained model for amorphous silica nanoparticles with parameters derived via potential matching to atomistic nanoparticle data, thus enabling large-scale simulations of realistic models of silica nanoparticles. Interaction parameters are optimized to match a range of nanoparticle diameters in order to increase transferability with nanoparticle size. Analytical functions are determined such that interaction parameters can be obtained for nanoparticles with arbitrary coarse-grained fidelity. The procedure is shown to be extensible to the derivation of cross-interaction parameters between coarse-grained nanoparticles and other moieties and validated for systems of grafted nanoparticles. The optimization procedure used is available as an open-source Python package and should be readily extensible to models of non-silica nanoparticles.

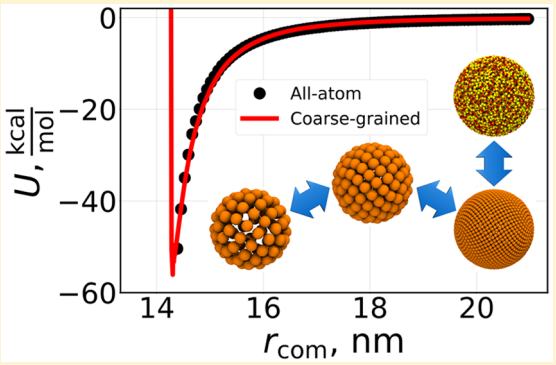

INTRODUCTION

Molecular simulations have played a critical role in providing an understanding of a wide range of phenomena related to nanoparticle systems,[1−11] with a large body of literature focused on the behavior of nanoparticles with oligomer/polymer coatings.[2,11−30] While systems can be examined with atomistic-level detail for very small nanoparticles, for example, molecular nanoparticles such as silsesquioxanes,[31−34] detailed atomistic simulations of even moderately sized systems become difficult, and even impractical, as nanoparticle size increases. In practice, atomistic simulations for even relatively small diameters (e.g., 5−10 nm) have been typically limited to a single or pair of nanoparticles due to the large number of atoms required to model these systems (e.g., ∼35,000 atoms for a nanoparticle of 10 nm diameter), especially when including solvent and/or coatings.[2,24] As a result, non-atomistic, coarse-grained (CG) models have been widely used to access the larger system sizes and longer time scales required to better understand nanoparticle behavior and more directly compare with experiment.

Many of the CG models used for nanoparticles are generic, often featuring simple functional forms, such as the Lennard-Jones (LJ) or square-well potentials, to model the interactions between nanoparticle cores or between subunits that describe a nanoparticle (e.g., beads used to construct generic rod-like,[35,36] cubic nanoparticles,[37] or spherical shells[38]). Often, these parameters are not tuned to experimental or atomistic data, and so the models are instead utilized to gather qualitative relationships between nanoparticle properties/behavior and features of the interactions (e.g., the depth of the potential well). While generic models are often highly effective at capturing such phenomenological behavior,[3,9,10,21,22] more specific models that attempt to recoup details of the underlying nanoparticle chemistry may be needed to more directly and accurately capture experimental behavior.

Although few models exist in the literature, several different approaches have been considered for developing chemically specific CG nanoparticle models. For example, accurate single-site CG C_{60} nanoparticle models have been constructed based on integrating the interactions between the underlying atoms in the nanoparticles, as in the work of Girifalco et al.,[39] and through the use of a force-matching comparison with atomistic molecular dynamics (MD) simulations, as in the work of Izvekov et al.[40] However, in single-site nanoparticle models, interactions are typically not transferable between different sizes, and thus a unique set of interactions must be derived for each nanoparticle size studied, including cross-interactions with solvent species and coatings. CG nanoparticles can also be constructed of smaller pseudoatoms (i.e., CG beads) with intermediate fidelity between all-atom and single-site models. Chan et al. developed a CG model of a polyoligomeric silsesquioxane (POSS) nanocube, including interactions with oligomer coatings, using the iterative Boltzmann inversion

Received: December 17, 2018
Published: March 27, 2019

DOI: 10.1021/acs.jctc.8b01269
J. Chem. Theory Comput. 2019, 15, 3260−3271

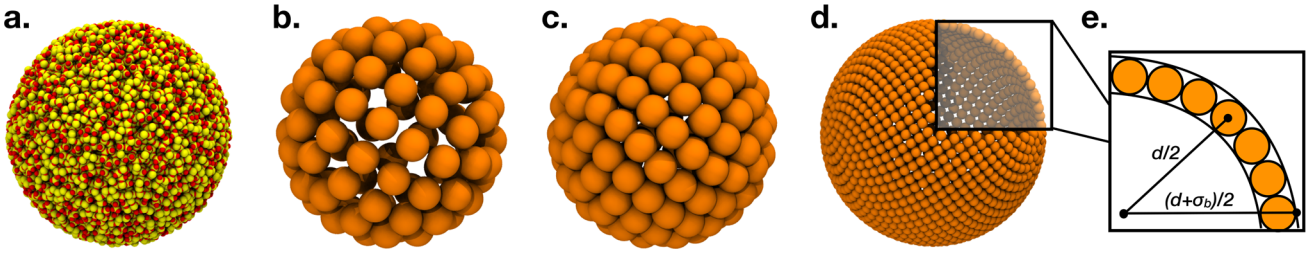

Figure 1. Amorphous silica nanoparticles (d = 10 nm) modeled using (a) an all-atom representation (carved as a sphere from an amorphous silica bulk; silicon is shown in yellow and oxygen in red) and CG representations featuring (b) σ_b = 1.5 nm, φ_b = 0.4, (c) σ_b = 1.5 nm, φ_b = 0.6, and (d) σ_b = 0.5 nm, φ_b = 0.6 (CG silica beads are shown in orange). The nanoparticles feature particle counts of (a) 34674, (b) 85, (c) 131, and (d) 1441, respectively. (e) A diagram of the spherical shell cross-section with a width equal to the pseudoatom diameter, σ_b. The volume fraction of pseudoatoms within the spherical shell is defined as φ_b.

method.[41] The silsesquioxane cube was represented by eight pseudoatoms (each pseudoatom represented a Si atom and half of each of the three O atoms it was bonded to), where the interactions of the pseudoatoms were optimized to match the radial distribution functions derived from corresponding atomistic simulations of POSS nanocubes. While this CG POSS nanocube model would likely be transferable to systems with other oligomer coatings, it is unclear whether the pseudoatoms in the nanocube could be effectively transferred to other silica nanoparticles, since the underlying chemical structure would be different (i.e., each Si in a POSS has three bonds with O, while most Si atoms in amorphous silica have four bonds with O) and the fact that the iterative Boltzmann inversion method often leads to potentials that are state/system specific.[42] Other approaches have specifically been designed to enable size-transferability, such that the underlying pseudoatoms do not need to change if the nanoparticle size is changed. For example, Lee and Hua developed a model for silica nanoparticles whereby nanoparticles were constructed of smaller CG pseudoatoms representing Si_6O_{12} subunits.[43] Si_6O_{12} clusters were chosen by Lee and Hua as they were found to best reproduce the density and heat capacity of amorphous silica when considering a range of Si_nO_{2n} substructures. The CG pseudoatom interactions were modeled using the LJ potential, optimized to reproduce the radial distribution function of a bulk atomistic simulation of Si_6O_{12}. While this approach yielded a CG model that could be transferred to different sized, and even different shaped, nanoparticles without rederivation, the CG nanoparticles were not directly validated to reproduce the energetic interactions between atomistically detailed amorphous silica nanoparticles. Additionally, in the approach of Lee and Hua, the fidelity of the pseudoatoms was fixed, which may impose practical limits on the maximum size of the nanoparticles that can be considered, as large nanoparticles would still feature a large number of interaction sites that could make their study computationally infeasible, even with a CG model.

Given the ubiquity of nanoparticles in experiment, it is of fundamental importance to develop a general approach for the optimization and validation of size-transferable CG nanoparticle potentials, along with cross-interaction parameters between nanoparticles and solvent/coating species, where the fidelity of the CG model can be adjusted. Herein, we introduce a general approach for the derivation of CG nanoparticles through the construction of a CG model for amorphous silica nanoparticles. Interactions are derived directly from all-atom nanoparticle models via a simplified version of the potential-matching scheme proposed by Toth,[44] and similar to the force-matching approach taken by Izvekov et al.[40] for C_{60}. Rather than using only a single nanoparticle size to perform the fitting, parameters are derived such that a single pseudoatom can simultaneously reproduce the behavior of a range of nanoparticle diameters, with the goal of increasing transferability of the CG model to different sized nanoparticles. For general applicability, pseudoatom interaction parameters are fitted to a Mie potential, allowing the shape and range to be tuned. The model does not prescribe a specific mapping (i.e., the all-atom equivalents to the CG beads are intentionally ambiguous), thus allowing the fidelity of the pseudoatoms to be tuned for the nanoparticle size of interest (see Figure 1). Furthermore, fits are applied such that parameters can be derived for nanoparticle models with arbitrary pseudoatom size and surface packing. Validation is performed by comparing against the target data and a range of systems not included in the optimization including larger nanoparticles, pairs of different sized nanoparticles, and interactions between spherical nanoparticles and dimers. The same potential-matching approach is utilized in the derivation of cross-interactions with linear alkanes, to enable further validation of the approach via the examination of polymer grafted nanoparticles. This validation is performed by comparing CG to all-atom models of the nanoparticles in the polymer grafted systems. The optimization framework is wrapped into an open-source Python package[45] to facilitate usage and extension by interested parties.

MODEL AND METHODS

Coarse-Grained Nanoparticle Model. CG nanoparticles were constructed using mBuild,[34] a package within the Molecular Simulation and Design Framework (MoSDeF).[46] The nanoparticle model consists of a spherical shell of pseudoatoms (i.e., CG beads), similar to the model of Lee and Hua[43] and In't Veld;[38] however, it should be noted that the pseudoatoms in our model are not defined to have a direct all-atom equivalent (see Figure 1). A golden section spiral algorithm is used to distribute these pseudoatoms in a roughly uniform distribution. Additional details on the golden section spiral algorithm can be found in the Supporting Information. The pseudoatom diameter is defined by σ_b, where σ_b is also used in the non-bonded interaction potential (eq 1). Thus, the model's resolution can be tuned by altering σ_b, where larger values result in a coarser nanoparticle model. The spherical shell is constructed such that each pseudoatom's center is placed at a distance of $\frac{1}{2}[d - (\sigma_b + \sigma_{silica})]$ from the nanoparticle center, where d is the diameter of the atomistic nanoparticle and σ_{silica} = 0.40323 nm is the arithmetic average

DOI: 10.1021/acs.jctc.8b01269
J. Chem. Theory Comput. 2019, 15, 3260−3271

of σ_{Si} and σ_O. This ensures that the van der Waals diameter of the nanoparticle remains nominally independent of the size of the pseudoatoms. Pseudoatoms are arranged at fixed values of φ_b, where φ_b represents the volume fraction of pseudoatoms within the spherical annulus described by $(d \pm \sigma_b)/2$, as depicted in Figure 1d, e. Thus, depending on the specified value of φ_b, pseudoatoms may feature a void space between neighboring beads (small φ_b, Figure 1b) or overlaps (large φ_b, Figure 1c, d).

Interactions involving the pseudoatoms of CG nanoparticles are governed by a potential with a Mie functional form:

$$U(r) = C\varepsilon\left[\left(\frac{\sigma}{r}\right)^n - \left(\frac{\sigma}{r}\right)^m\right] \quad (1)$$

where the prefactor C relates to the exponents n and m, where $C = \left(\frac{n}{n-m}\right)\left(\frac{n}{m}\right)^{m/n-m}$. For interactions between pseudoatoms, σ in eq 1 is equivalent to σ_b, while for cross-interactions between pseudoatoms and other moieties, σ is included in the optimization. Preliminary work revealed codependency between the parameters ε, n, and m in eq 1, supporting the concept of Mie potential degeneracy that has been noted elsewhere in the literature.[47] As such, for all interactions (both those between pseudoatoms and all cross-interactions), the value of n has been fixed at 35, which was found to provide reasonable parameter sets and helps capture the excluded volume of the nanoparticle core. However, the parameters ε and m are dependent on the values of σ_b and φ_b used to construct a given nanoparticle. The work herein describes the optimization of these two parameters, such that the collective interaction between the pseudoatoms of two nanoparticles matches data obtained for atomistically detailed nanoparticles.

Atomistic Target Data. Atomistic nanoparticles were constructed by carving spheres from an amorphous silica bulk. Bulk amorphous silica was generated using a procedure that closely mimics the approach of Litton and Garofalini[48] however with the ReaxFF force field[15] to describe Si and O interactions,[49] as in the work of refs 50 and 51. Briefly, a 5 nm × 5 nm × 5 nm simulation box was filled with a stoichiometric mixture of Si and O atoms at a density of 2.2 g/mL and heated to 10,000 K over 20 ps to obtain a fluid. Stepwise annealing was performed to cool the system to room temperature, through 10 ps isothermal-isochoric runs at 8000, 6000, 4000, 3000, 2000, 1000, and 300 K. A 0.5 fs time step was used, and charge equilibration was performed at each time step, making use of the implementation by Aktulga et al.[52] Temperature was controlled using a Nose-Hoover thermostat[53,54] (with a damping parameter of 100 fs) using the LAMMPS MD simulation engine.[55,56]

Nanoparticles were carved from the bulk amorphous silica by including all atoms within a spherical region of a specified diameter (See Figure S3 in the Supporting Information). Figure 1a shows the result of this procedure for a nanoparticle with a diameter of 10 nm. The silica bulk was replicated when necessary for the creation of large nanoparticles (See Figure S3 in the Supporting Information). Note that although a strict 2:1 stoichiometric ratio of oxygen atoms to silicon atoms was not enforced when carving the nanoparticles (although the bulk is stoichiometric, so these values are close), the force field chosen to evaluate nanoparticle−nanoparticle interactions did not include partial charges (discussed later), so there were no concerns with charge neutrality. More rigorous models allowing for the presence of an outer oxygen layer (mimicking expected oxidation) and relaxation of the nanoparticles to form slightly aspherical shapes were also examined; however, it was found that the inclusion of these more detailed features did not appreciably alter the nanoparticle−nanoparticle interaction energy (see Figures S4 and S5 in the Supporting Information), and thus they were excluded for computational efficiency. Scripts for initializing all-atom nanoparticles are provided in the open-source Python package associated with this work.

Force field parameters for silicon and oxygen, used in calculating the interaction potential between atomistic nanoparticles, were obtained from the hybrid COMPASS force field,[57,58] which has been shown to yield good agreement in thermophysical properties with experiment for systems of silica nanoparticles.[59] Further details on the choice of the hybrid COMPASS force field and a comparison to the OPLS and DREIDING force fields for the calculation of nanoparticle−nanoparticle interaction potentials can be found in the Supporting Information (see Figure S6a), where we note the hybrid COMPASS and DREIDING force fields are almost indistinguishable and OPLS predicts the same shape of the interaction, but shifted to slightly smaller separations.

Non-bonded interactions are defined by a 9-6 Class2 LJ-like potential:

$$U(r) = \varepsilon_{ij}\left[2\left(\frac{\sigma_{ij}}{r}\right)^9 - 3\left(\frac{\sigma_{ij}}{r}\right)^6\right] \quad (2)$$

and sixth-order mixing rules[60] are used for cross-interactions (see eqs S1 and S2 in the Supporting Information). Atoms do not feature partial charges, as previous work has shown partial charges to have a negligible impact on thermophysical properties in similar systems,[59] and their exclusion aids in the reduction of computational cost. Additional information concerning the role of partial charges on nanoparticle−nanoparticle interaction energy is included in Figure S6b of the Supporting Information. Note, the interaction energy was calculated between isolated pairs of nanoparticles (i.e., periodic boundary conditions were not considered), and no interaction cutoff was employed.

Target data were obtained for nanoparticles with diameters of d = 4, 6, 8, 10, 12, 14, 16, 18, and 20 nm. To gauge transferability of the CG modeling approach to larger nanoparticles sizes, data were also collected for an all-atom nanoparticle with a diameter of 50 nm. Additionally, interaction potential data were collected between dissimilar sized nanoparticles (with diameters of 8 and 16 nm) and between a spherical nanoparticle and a dimer (consisting of two adjoining nanoparticles).

Energy profiles were obtained by binning interaction energy values into histograms over a range of center-of-mass separations, using a consistent number of 100 bins (providing higher resolution for smaller nanoparticles); interactions were calculated for $r_{com} < d + 3 + \text{ceil}(d/4)$. An even sampling was performed across the entire range of interparticle separations, although it should be noted that the larger nanoparticles featured reduced sampling as variability in interaction potential at a given separation is reduced for the particles of larger size; this also reduces the computational cost. Sampling involved iteratively choosing random rotations and translations for one of the two nanoparticles such that the final energy profiles yielded an average over many configurations within each bin. An overlap criterion was applied, such that configurations

DOI: 10.1021/acs.jctc.8b01269
J. Chem. Theory Comput. 2019, 15, 3260−3271

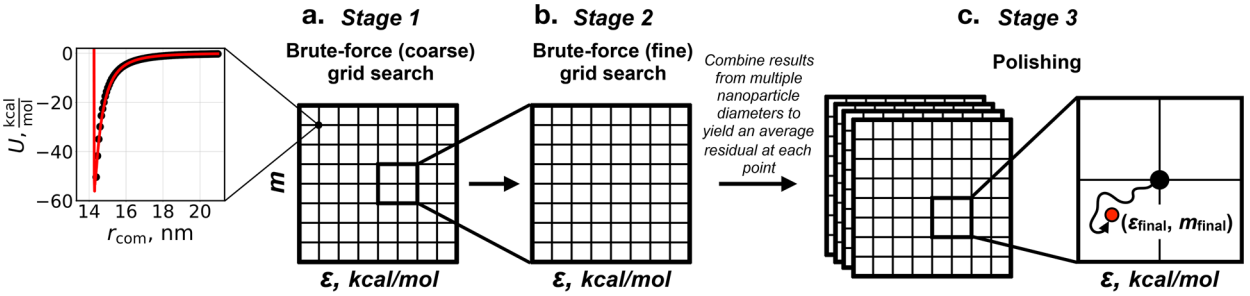

Figure 2. Overview of the workflow for optimizing CG nanoparticle parameters.

featuring any two atoms closer than 0.8σ were excluded; we note that rejected configurations were not counted toward our uniform sampling. However, it was ultimately found during the optimization of the pseudoatom interactions that overlaps in the regime of smaller center-of-mass separations prevented reasonable fits. The data were then pruned to remove values at center-of-mass separations below d + 0.40323 nm × 0.8, where 0.40323 nm represents the arithmetic mean of Si and O diameters, to resolve this issue. Additional details on the sampling procedure are provided in the Supporting Information.

Target data were also collected for the interaction between an atomistic nanoparticle with d = 10 nm and united-atom (UA) alkane moieties. Specifically, the interaction potential was calculated over a range of center-of-mass separations between the atomistic nanoparticle and both CH_2 and CH_3 pseudoatoms. The collection of nanoparticle-alkane target data followed the same procedure as that used for collecting the nanoparticle−nanoparticle target data; however, bin spacing was reduced in the region of the potential well to provide better definition. Specific details are available in the Supporting Information. Interactions between silica and UA pseudoatoms featured a 12-6 LJ potential with parameters obtained from Ionescu et al.[33] who followed the work of Frischknecht and Curro.[59,61] While the error in the target data was found to be large at low separations, it was found that the inclusion of data points on both sides of the potential minimum was necessary to yield a proper fit. Target data were sanitized to ensure, from low to high separations, that interaction potentials were monotonically decreasing until the potential minimum and monotonically increasing afterward (removing data points that did not fit this criterion).

Alkane-Grafted Nanoparticles. Alkane-grafted nanoparticles are considered in this work as a means of validating the force field derivation process and demonstrating its utility. For both all-atom and CG nanoparticle models, chains are placed in an evenly distributed spherical array (again using a golden section spiral algorithm), extending normal to the nanoparticle surface. Chains are attached to the nanoparticle core by fixing the terminal polymer bead closest to the nanoparticle and treating the entire unit of the core plus these terminal beads as a singular rigid body, that is, no physical bonds are defined between the chains and the nanoparticle core, allowing for a more direct comparison between atomistic and CG nanoparticle models. A dense surface chain density of 3.0 chains/nm^2 is used in this study.

Nanoparticle cores are modeled using both atomistic and CG representations, constructed using the procedures outlined in the preceding sections. Polymer grafts feature a UA representation for both CG and atomistic models, where interactions between polymer chains are described by the TraPPE force field[71] and cross-interactions with the all-atom core are obtained from Ionescu et al.[59] Interactions between UA polymer grafts and pseudoatoms of CG nanoparticle cores take the form of eq 1 and are derived through a potential-matching approach analogous to that used to obtain interactions between the CG nanoparticle cores themselves, as described in further detail in the Parameterization of Cross-Interactions section. Note that the only difference between CG and atomistic systems is the nanoparticle core, allowing the quality of the derived CG interactions to be directly tested (i.e., chain arrangements and chain−chain interactions do not change). Simulations of alkane-grafted nanoparticles are performed using the HOOMD-blue simulation engine.[62,63] Single alkane-grafted nanoparticles with chain lengths of 12, 24, 36, and 72 carbons are considered, where integration is performed only on the alkane tethers (excluding the end beads closest to the nanoparticle core). The presence of an implicit solvent is accounted for by truncating chain−chain interactions at the potential minimum (thus leading to a purely repulsive interaction) and through integration using Langevin dynamics, in a manner similar to that of Peters et al.[2] It should be noted that in this work, the interactions between the nanoparticle and chains are *not* truncated at the potential minimum, so as to provide a means of validating the cross-interaction parameters (nanoparticle−chain interactions are instead truncated at 2.0 nm for systems featuring an all-atom nanoparticle and at 2.0 nm + $\sigma_b/2$ for systems featuring a CG nanoparticle, where we note that this cutoff fully captures the interaction range of this interaction). Following a brief energy minimization, systems are equilibrated for 10 ns, the final 2 ns of which are used for sampling. Simulations are performed at a temperature of 300 K and use a time step of 2 fs.

As shown in Figure 1b, c, CG nanoparticle models may feature a void space between the beads, particularly at low values of φ_b, which may cause issues with the intercalation of chain particles into the nanoparticle core. To prevent this in our grafted nanoparticle systems, a short-range repulsive potential is utilized radiating from the nanoparticle center featuring a 12-6 LJ potential with ε = 5 kcal/mol and both σ and r_{cut} equal to the nanoparticle radius. This was found to be sufficient to prevent the intercalation of chain particles into the nanoparticle core, with minimal impact on film structure.

Force-Field Optimization. Derivation of pairwise interactions between CG pseudoatoms is achieved through potential matching, whereby parameters in eq 1 are optimized such that the collective interaction potential between two CG nanoparticles as a function of the center-of-mass separation matches the corresponding results from all-atom nanoparticles, through minimization of the residual:

DOI: 10.1021/acs.jctc.8b01269
J. Chem. Theory Comput. 2019, 15, 3260−3271

$$e = \sum \frac{|U_{aa}(r_{com}) - U_{cg}(r_{com})|}{|U_{aa}(r_{com})| + |U_{cg}(r_{com})|} \quad (3)$$

where U_{aa} and U_{cg} represent the nanoparticle−nanoparticle interaction potential for the all-atom and CG models, respectively, at a given center-of-mass separation, r_{com}. Normalization is used to provide an even weighting of the energy scales across all values of r_{com}. We use the term "interaction potential" in place of the more common "potential of mean force" as potential values for each center-of-mass distance are not Boltzmann weighted; however, these values are shown to feature negligible orientational dependence. Figure 2a shows the all-atom interaction potential for nanoparticles with d = 7 nm overlaid by results from the CG model for σ_b = 1.0 nm and φ_b = 0.5.

A Python package has been developed to perform these optimizations that relies on tools available from the scientific Python stack (most heavily SciPy),[64] mBuild,[34] and is hosted on GitHub,[45] with usage examples provided on GitHub and in the Supporting Information. Optimizations are performed via the following multistage process (outlined in Figure 2):

(1) A brute-force optimization over a coarse multidimensional grid spanning a wide parameter range. Each point on the grid represents a different nanoparticle state, defined by the values of d, σ_b, and φ_b (see Figure 2a).
(2) A second brute-force optimization over a fine multidimensional grid spanning a narrower parameter range. Here, the ranges of d, σ_b, and φ_b are reduced for the nanoparticle states considered (see Figure 2b).
(3) A polishing stage. The starting point for this stage is chosen from the results of the second brute-force optimization for a range of nanoparticle sizes (to ensure the creation of a transferable parameter set). A final optimization is performed from this starting point using a Nelder−Mead simplex algorithm (see Figure 2c).[65,66]

Initial attempts at optimization included only Stage 3 and led to traps in local minima. As a result, Stage 2 was added to provide a greater likelihood that the global minimum is reached. Stage 1 was added such that optimized parameter sets could be generated without the need to hand-pick parameter bounds for each set. Nanoparticle diameters of d = 4, 6, 8, 10, 12, 14, 16, 18, and 20 nm are considered in the optimizations. To yield a parameter set that is transferable across a range of nanoparticle diameters, these diameters are considered simultaneously in Stage 3 of the optimization, where the total residual simply becomes the sum of the individual residuals for each nanoparticle diameter.

PARAMETERIZATION OF NANOPARTICLE−NANOPARTICLE CORE INTERACTIONS

Interaction parameters between CG pseudoatoms, as defined by eq 1, are inherently dependent on the diameter of the CG beads (i.e., σ_b). These parameters will additionally be dependent on the volume fraction of beads included within the spherical annulus (i.e., φ_b). Furthermore, discrete parameter sets could be obtained for different nanoparticle sizes (i.e., d). However, such parameter sets would limit the scope and usability of the force field. Here, our goal is to define a force field where parameters may be obtained for nanoparticles featuring arbitrary values of d, σ_b, and φ_b. Independence of d is achieved, as described in the preceding section, by including data from many nanoparticle sizes in Stage 3 of the optimization (Figure 2c). Additionally, to support arbitrary values of σ_b and φ_b, parameters should be derived as *functions* of these two variables. This is achieved by performing Stages 1 and 2 of the optimization scheme for 1010 different nanoparticle states (i.e., d, σ_b, and φ_b), with ranges of d = 4−20 nm, σ_b = 0.5−2.0 nm, and φ_b = 0.25−0.60. Additional details on the states included in the optimization can be found in the Supporting Information. Stage 3 of the optimization (the polishing stage) was performed for each σ_b and φ_b combination, including data from multiple radii simultaneously.

For the two parameters included in the optimization, ε and m, the results of Stage 3 for each value of φ_b were examined as a function of σ_b, as shown in Figure 3a, b. From Figure 3a, it is

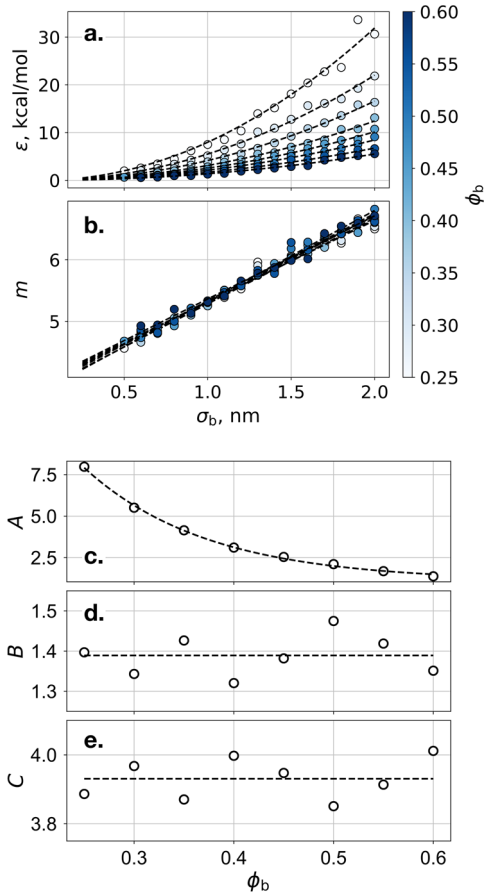

Figure 3. Optimized (a) ε and (b) m values as a function of σ_b. Dashed lines represent (a) exponential and (b) linear fits to the data. In plots (c−e), values for the fitting parameters A, B, and C are, respectively, shown as functions of φ_b. Dashed lines represent (c) exponential and (d-e) constant fits to the data.

observed that ε increases as σ_b is increased. This result is expected, as nanoparticles featuring larger bead sizes will also feature a lower total number of beads, thus ε must increase to yield the same collective interaction energy. Likewise, ε is found to increase as φ_b is decreased, along similar reasoning. Figure 3b shows that as σ_b increases, m also increases. This reflects a softening of the potential as the nanoparticle model becomes further CG. Interestingly, m is found to be independent of φ_b, as Figure 3b shows all curves collapse onto a single line. From Figure 3a, b, it appears that ε features

DOI: 10.1021/acs.jctc.8b01269
J. Chem. Theory Comput. 2019, 15, 3260−3271

a quadratic dependence on σ_b, while m features a linear dependence. As such, the following general equations can be used to describe ε and m as a function of σ_b:

$$\varepsilon = A\sigma_b^2 \quad (4)$$

$$m = B\sigma_b + C \quad (5)$$

Figure 3c–e shows the φ_b-dependent coefficients A, B, and C from eqs 4 and 5 obtained for discrete values of φ_b by performing fits to the data in Figure 3a, b. Both quadratic and exponential functions are found to provide good fits to the data for A shown in Figure 3c, where A is shown to decrease (and thus ε is reduced) as φ_b increases. However, the fit using an exponential function was slightly better than using a quadratic function, so this function was chosen to obtain the coefficient A as a function of φ_b. As expected from the results shown in Figure 3b, the coefficients B and C from eq 5 appear from Figure 3d, e to be independent of the value of φ_b. As a result, these coefficients can be obtained by taking a simple average of the values obtained for the various values of φ_b. From these fits, ε and m can be described in terms of σ_b (in units of nm) and φ_b through the following relations:

$$\varepsilon(\text{kcal/mol}) = (51.417 \times e^{-8.081\varphi_b} + 1.095)\sigma_b^2 \quad (6)$$

$$m = 1.389\sigma_b + 3.931 \quad (7)$$

Using these relations, values for ε and m can be generated for arbitrary values of σ_b and φ_b.

Figure 4 shows the nanoparticle–nanoparticle interaction energy obtained for atomistic nanoparticles compared to that

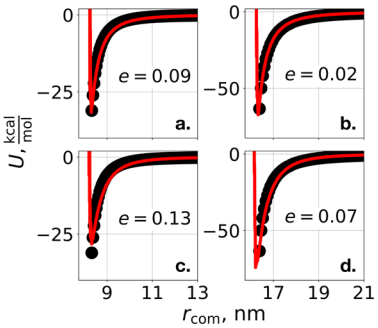

Figure 4. Interaction energy profiles calculated between nanoparticles with (a) d = 8 nm, σ_b = 0.8 nm, φ_b = 0.3, (b) d = 16 nm, σ_b = 0.8 nm, φ_b = 0.3, (c) d = 8 nm, σ_b = 1.6 nm, φ_b = 0.6, and (d) d = 16 nm, σ_b = 1.6 nm, φ_b = 0.6. Circles represent all-atom data, while lines represent results for CG nanoparticles with parameters derived from eqs 6 and 7. The residual of the energy, e, calculated using eq 3 is included for each subplot, where a value of e = 0 corresponds to an ideal match.

calculated between CG nanoparticles using the results of eqs 6 and 7. It is shown that the CG results compare reasonably well to the all-atom data for several combinations of σ_b and φ_b. These fits are especially good in the long-range region, which is of particular importance as nanoparticles will typically feature some sort of surface coating in practical simulations, which will nullify the effects of the short-range region. The quality of the fits does appear to feature some dependence on the nanoparticle size as well as σ_b and φ_b, which is explored further in the following section. However, the overall results suggest that CG nanoparticles with parameters derived from eqs 6 and 7 are able to achieve good comparison in interaction energy to the all-atom models, with the slight deviations outweighed by the advantages of the utility of these equations.

Transferability. The goal of the derivation of eqs 6 and 7, relating ε and m from eq 1 to σ_b and φ_b, was to obtain functions that could be used across a wide range of σ_b, φ_b, and d values. To test the transferability of these functions, parameters obtained using these equations were used to calculate the interaction energy between CG nanoparticles, and the result was compared to all-atom data using eq 3. Figure 5 shows these results in the form of heatmaps for various σ_b and φ_b values for nanoparticles with diameters of 8, 12, and 16 nm. From Figure 5, it is found that the parameters obtained from eqs 6 and 7 describe nanoparticles with a wide range of different σ_b, φ_b, and d values well. Interestingly, the normalized value d/σ_b appears to have very little influence on the performance of these parameters. Additionally, the ability for the CG model to fit to the all-atom data appears to be independent of φ_b. As a result, the fit seems only dependent on the value of σ_b itself, where fits are found to be worse when σ_b < ~0.45 nm (see Figure 5a) and when σ_b > ~3.0 nm (see Figure 5c). The poor fits for low values of σ_b are likely due to its similarity in size to the "diameter" of silica itself (0.40323 nm, from earlier). As such, the "CG" model approaches the same length scale as the atomistic model, and features of the atomistic model that could be averaged into larger CG pseudoatoms are not well-described by the smaller beads. On the other end of the spectrum, the poorer fits that begin to occur as σ_b increases beyond 3.0 nm are likely a simple result of the reduced fidelity of the model, although it should still be noted that residual values are <0.2 even at $\sigma_b \approx$ 3.2 nm. In this regime of σ_b > 3.0 nm, the model becomes more and more CG and with this comes some loss of accuracy. Furthermore, as these σ_b values are larger than any included in the target data for the optimization, any error in the fitting will become increasingly pronounced as σ_b increases further beyond the target data limit.

Figure 6a shows the residuals calculated using eq 3 from all-atom data for a nanoparticle where d = 50 nm (not used in the optimization) and CG data for various values of σ_b and φ_b, in order to test the size transferability of the derived parameters to larger nanoparticles. As might be expected, the error is higher than for the smaller nanoparticles used in obtaining the parameters; however, there are clear regions where the parameters from eqs 6 and 7 perform well, particularly for values of φ_b = 0.36. The lowest residual (e = 0.06) is observed where σ_b = 3.17 nm and φ_b = 0.36, and a comparison between the interaction energy profile between nanoparticles constructed using these values with the all-atom system is shown in Figure 6b, visually demonstrating good agreement. Also shown in Figure 6b are interaction energy profiles for several other combinations of σ_b and φ_b to provide a sense of the sensitivity to these parameters. The error for these systems is nearly independent of σ_b, and instead is highly dependent on φ_b. As shown in Figure 6b, slight increases or decreases in φ_b (±0.05) from the optimal value (0.36) result in significant deviations in the depth of the potential well as well as the shape of the curve. However, increasing σ_b from 3.17 to 6.5 nm results in only a slight change in the interaction potential curve. Interestingly, the region in Figure 6a, where the error is lowest, corresponds closely to be the asymptotic value found for φ_b, as the nanoparticle radius is increased for nanoparticles constructed in a manner of maximum packing (where the largest number of pseudoatoms are used to construct

DOI: 10.1021/acs.jctc.8b01269
J. Chem. Theory Comput. 2019, 15, 3260–3271

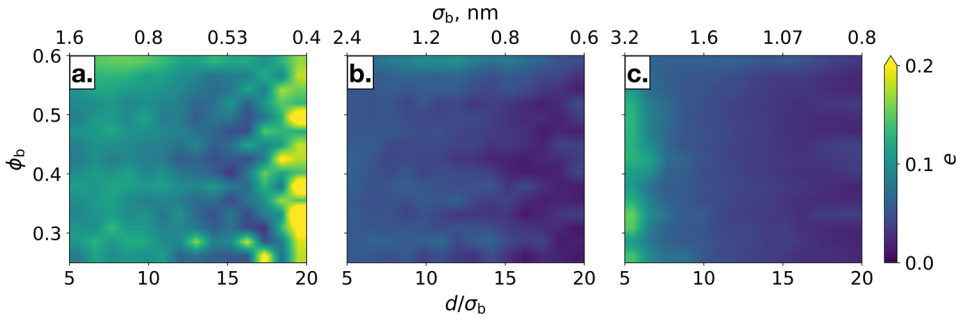

Figure 5. Heatmaps showing the interaction energy residual from eq 3 as a function of CG particle size (represented by the normalized and absolute values d/σ_b and σ_b, respectively) and φ_b for nanoparticles with diameters of (a) 8 nm, (b) 12 nm, and (c) 16 nm.

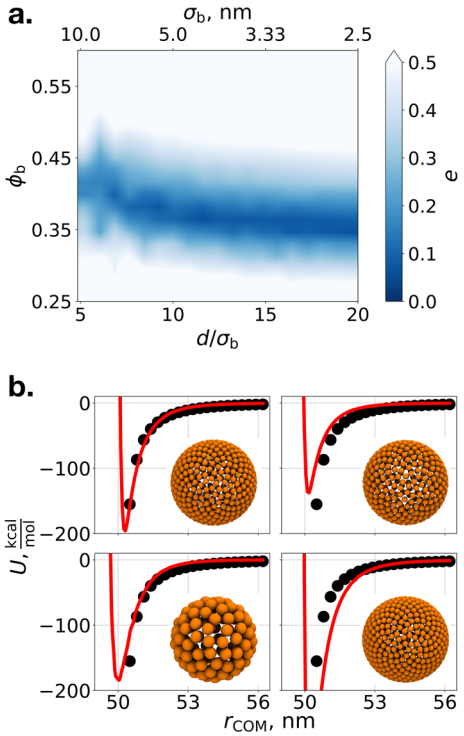

Figure 6. (a) Heatmap showing the interaction energy residual from eq 3 as a function of CG particle size (represented by the normalized and absolute values d/σ_b and σ_b, respectively) and φ_b between nanoparticles with d = 50 nm, and (b) a comparison of the all-atom interaction energy profile (black circles) with that of CG nanoparticles (red lines) constructed using (clockwise starting from the top-left) σ_b = 3.17 nm, φ_b = 0.36 (corresponding to the lowest residual in the heatmap, e = 0.07), σ_b = 3.17 nm, φ_b = 0.31 (e = 0.29), σ_b = 3.17 nm, φ_b = 0.41 (e = 0.27), and σ_b = 6.5 nm, φ_b = 0.36 (e = 0.17). Snapshots of each of the CG nanoparticles are also provided.

nanoparticles without overlaps, see Figure S1 in the Supporting Information). This suggests that the presence of overlaps between beads at high values of φ_b and gaps between beads at low values of φ_b may present issues with transferability for larger nanoparticle sizes, which may be related to the reduced curvature of the large particle. As such, Figure 6 suggests accurate interaction potential curves can be constructed over a wide range of nanoparticle sizes for our CG model, where it appears a value of φ_b around 0.36 provides the highest accuracy as a diameter increases.

To this point, all interaction energies considered have been between two nanoparticles that each feature the same diameter and same level of pseudoatom fidelity. Figure 7a–c shows a comparison of all-atom and CG data for the interaction potential between two nanoparticles, where one nanoparticle has a diameter of 8 nm, σ_b = 0.6 nm, and φ_b = 0.4, while the other nanoparticle features a diameter of 16 nm, φ_b = 0.5, and σ_b = 0.6, 1.3, or 2.0 nm. The all-atom data shown in this figure were not included in any optimization and are present for comparison only. Cross interactions between the two nanoparticles were obtained using geometric mixing rules for σ and ε and an arithmetic mixing rule for m. Figure 7a, b reveals excellent fits between the CG and all-atom data, while Figure 7c shows some deviation, although the CG and all-atom potential curves still share the same general features. This supports the use of the model derived herein for systems of nanoparticles with different sizes and mixed fidelities. Additional comparisons, shown in Figure S7 of the Supporting Information, reveal fits to be nearly independent of φ_b.

It is of additional interest to consider how the model herein may apply to systems of anisotropic nanoparticles. As a simple test, interactions between a single nanoparticle (d = 10 nm, σ_b = 1.3 nm, φ_b = 0.4) and a dimer (composed of two neighboring spherical nanoparticles, roughly estimating a fused nanoparticle) have been examined and are shown in Figure 7d–f. The interaction energy between these two nanoparticles has been considered for three different dimer orientations, and a comparison has been made between the all-atom model and the CG model with parameters derived in this work. Excellent agreement is observed between these two models, suggesting the transferability of the CG parameters to non-isotropic nanoparticles. It should be noted that both entities in this comparison feature curved surfaces; consideration of nanoparticles featuring vertices or flat faces is outside the scope of the current study.

PARAMETERIZATION OF CROSS-INTERACTIONS

The same general potential-matching procedure outlined in Figure 2 can also be used to derive interactions between CG nanoparticles and other species (e.g., atom types/moieties from existing polymer force fields). This becomes powerful as it facilitates use of the CG silica model presented in this work beyond simple systems of silica nanoparticles in vacuum and allows for more complex systems such as polymer-grafted nanoparticles and nanoparticles in a solvent. While the use of Mie mixing rules could be one approach to obtaining these cross interactions, large differences in both σ_b and the exponent values would likely result in poor accuracy.

Table 1 shows parameters obtained for the interaction between pseudoatoms of a CG nanoparticle (σ_b = 1.3 nm, φ_b = 0.4, d = 10 nm) and both CH_2 and CH_3 UA moieties. Note that the parameters in Table 1 are not guaranteed to be

DOI: 10.1021/acs.jctc.8b01269
J. Chem. Theory Comput. 2019, 15, 3260−3271

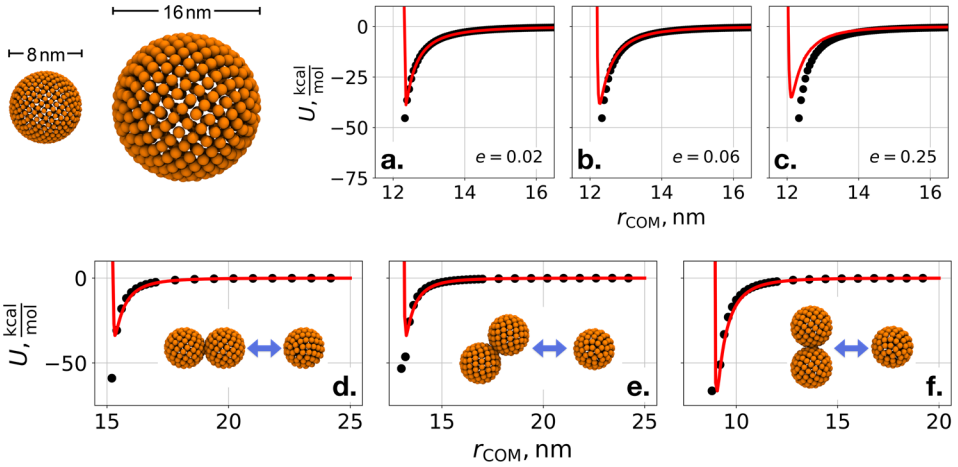

Figure 7. Interaction potential between a nanoparticle with d = 8 nm, σ_b = 0.6 nm, and φ_b = 0.4 and a nanoparticle with d = 16 nm, φ_b = 0.5, and (a) σ_b = 0.6 nm, (b) 1.3 nm, and (c) 2.0 nm. Also shown are interaction potentials between a nanoparticle with d = 10 nm, σ_b = 1.3 nm, and φ_b = 0.4 and dimers constructed of two attached nanoparticles with these same parameters rotated at angles of (d) 0°, (e) 45°, and (f) 90°. Points represent all-atom data, and lines represent CG data using parameters obtained from eqs 6 and 7 and the mixing rules detailed in the main text.

Table 1. Optimized Interaction Parameters between CG Nanoparticle Beads (σ_b = 1.3 nm, φ_b = 0.4) and CH_2, CH_3 UA Beads

cross-interaction	σ (nm)	ε (kcal/mol)	n	m
NP-CH_2	0.7581	1.2809	35	6.9256
NP-CH_3	0.7435	1.6871	35	6.3843

transferable to CG nanoparticles with arbitrary values of σ_b, φ_b, and d. Our focus here is to demonstrate how cross-interactions with other particle types can be obtained rather than the presentation of a more general cross-interaction parameter set. The parameters in Table 1 provide an excellent match to the all-atom target data for the two cross-interactions, as shown in Figure 8. As in Figure 4, target data for long-range interactions

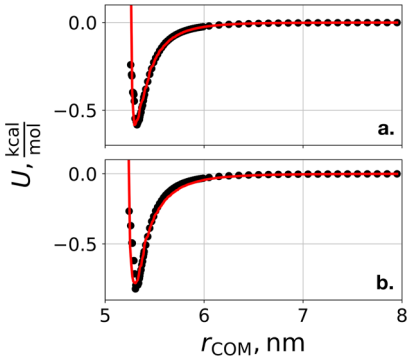

Figure 8. Interaction energy profiles calculated between a nanoparticle with d = 10 nm and (a) CH_2 and (b) CH_3 UA moieties. Circles represent all-atom target data, while lines represent results for CG nanoparticles with σ_b = 1.3 nm and φ_b = 0.4.

have been included to ensure this portion of the potential curve is properly captured in the CG model. Additionally, as the cross-interactions feature a (relatively) softer potential compared to the interactions between the pseudoatoms of nanoparticle cores, target data were also able to be obtained for the interaction at short-range, providing definition to the potential well. It was found that the inclusion of this short-range data was essential in the derivation of cross-interactions with a properly located potential minimum.

To validate the interactions in Table 1, alkane-grafted nanoparticles are constructed with both all-atom and CG cores and where the alkane coating is allowed to reach a steady state; the radial mass density profiles of the chains are calculated as a measure of parameter effectiveness. Figure 9 shows the radial

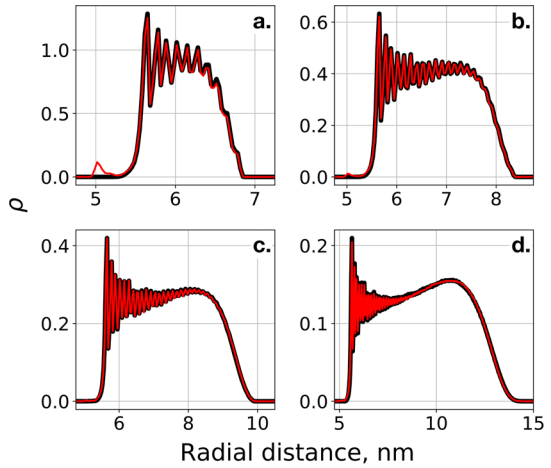

Figure 9. Radial mass density (ρ) of alkane tethers with chain lengths of (a) 12, (b) 24, (c) 36, and (d) 72 carbons attached at a density of 3.0 chains/nm^2 to a silica nanoparticle with d = 10 nm. Results obtained for an all-atom nanoparticle core are shown in black, while results for a CG core (using parameters from Table 1 with σ_b = 1.3 nm) are shown in red. Contributions to ρ from the two CH_2 beads closest to the nanoparticle surface (the nearest most of which has a fixed position) are excluded for clarity.

mass density profiles for nanoparticles with alkane grafts featuring chain lengths of 12, 24, 36, and 72 carbons. It can be observed that for all chain lengths, the systems with the CG nanoparticle core closely match the film structure of those with an all-atom core, with the results nearly indistinguishable. The potential curves are found to become smoother further from the nanoparticle surface (most evident in Figure 9d.), as the radial volume increases. At distances near the nanoparticle surface, the available volume for chains to explore is quite low,

DOI: 10.1021/acs.jctc.8b01269
J. Chem. Theory Comput. 2019, 15, 3260−3271

particularly at a high chain density of 3.0 chains/nm^2, and large peaks are present indicating the locations of individual CH_2 moieties along the chain backbone. These features of the mass density profiles are well-captured by the CG model. The only notable difference between the film structures of the two models is a small peak located near the nanoparticle surface (at a radial distance of 5 nm) that is present for the C12 and C24 coatings shown in Figure 9a, b. This peak corresponds to chains that have intercalated into regions between neighboring pseudoatoms of the CG nanoparticle core. While a pseudo hard-sphere potential is utilized to prevent chains from intercalating into the nanoparticle itself (which as discussed previously would otherwise be possible as a result of "gaps" between neighboring pseudoatoms, see Figure 1d), this does not prevent chains from exploring the region around the nanoparticle surface that is made rough by the large size of the pseudoatoms. However, this effect is shown to be quite minor in Figure 9 with little effect on the overall film structure and becomes unnoticeable at chain lengths of 36 and 72 carbons.

DISCUSSION

The model and associated force field presented herein for CG silica nanoparticles provide a means to create systems of amorphous silica nanoparticles with user-specified fidelity. Cross-interactions with particles from other force fields are also obtainable through the same potential-matching approach. However, while the utility of such a generalized force field should not go unstated, a comparison with the existing silica force field of Lee and Hua[43] is also useful. Figure 10 shows a comparison of the nanoparticle−nanoparticle interaction potential between CG nanoparticles using parameters from eqs 6 and 7 and between point-particles using parameters obtained from the work of Lee and Hua (the exact equations and parameters used are provided in the Supporting Information), alongside the atomistic nanoparticle data calculated in this work. The parameters from this work yield a CG nanoparticle−nanoparticle interaction potential that closely matches the shape of the all-atom data, which is to be expected as atomistic data were used to fit these parameters. Comparing to the potential curve obtained using parameters from the work of Lee and Hua, both potentials provide a similar value for the well depth, however, the Lee and Hua potentials show a much sharper character, particularly for larger nanoparticle diameters, where the interaction potential increases to nearly zero at a center-of-mass separation of only 1 nm beyond the nanoparticle diameter. This shorter-range behavior in the Lee and Hua potential is likely related to the use of the 12-6 LJ potential to model the pseudoatom interactions. From eq 6, our work predicts that for a pseudoatom with a matching diameter to Lee and Hua (0.62 nm), the attractive exponent of the Mie potential corresponds to a value of 4.79 (note this appears independent of the surface density of the pseudoatoms), resulting in longer-ranged interactions than the standard 12-6 potential. This lack of long-range attraction may have effects on the dynamics, assembly, and supra-molecular structure of bulk systems. Furthermore, it is important to note that, although the magnitude of the interaction potential in this long-range region is small relative to that at short-range, these values may still be quite large relative to interactions between other constituents in the system. For example, considering the grafted alkane example, if a standard interaction cutoff of $1/60\varepsilon$ were to be applied to the interaction between pseudoatoms that make up the nanoparticle core particles for d = 10 nm, the nanoparticle−nanoparticle interaction energy would be truncated at a value on the order of 1 kcal/mol. We note that this is on the same energy scale as the well depth of the nanoparticle−CH_x interaction (shown in Figure 8) and an order of magnitude larger than the well depth of the CH_x−CH_x interaction (~0.1 kcal/mol). Again, this considerable heterogeneity in the energy scales could result in significant changes to the dynamics, assembly, and structure of the systems if cutoffs are not appropriately chosen to capture this longer-range behavior.

Finally, an additional advantage of the model and force field presented herein that should be discussed is the ability to derive cross-interactions between polymer pseudoatoms for which no all-atom interaction parameters are available. As an example, consider a CG alkane with a 3:1 mapping, (3 CH_2/CH_3) units mapped into a single bead. While several such force fields exist,[42,67−70] to the best of our knowledge, none contain interaction parameters with silica nanoparticles. In the approach presented herein, one could use as target data the interaction between, for example, a CH_2−CH_2−CH_2 trimer that forms the underlying structure of the CG bead and an all-atom nanoparticle core and then simply fit the parameters for the interaction between a CG core and a CG alkane moiety to this target data, similar to the united atom alkane examples. As a result, any polymer that can be mapped to the atomistic level is compatible with the CG nanoparticle model presented and the procedure.

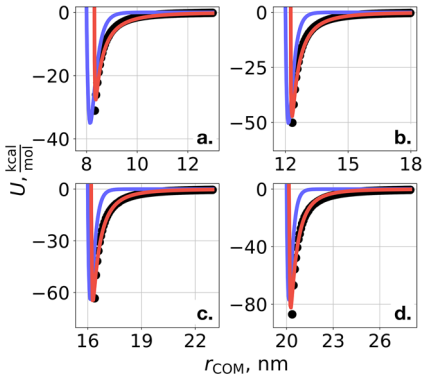

Figure 10. Interaction energy profiles calculated between nanoparticles with diameters of (a) 8 nm, (b) 12 nm, (c) 16 nm, and (d) 20 nm. Data are shown for nanoparticles featuring all-atom representations (black circles), the CG model described in this text with d/σ_b = 12.5 and φ_b = 0.5 (red lines), and parameters from Figure 6 of ref 43 (blue lines).

CONCLUSION

In this work, a CG force field has been derived for amorphous silica nanoparticles, modeled as spheres of evenly distributed pseudoatoms, via matching interaction potentials to all-atom data. The optimization scheme considers target data for multiple nanoparticle sizes simultaneously to yield parameters that are size independent. Interactions between pseudoatoms utilize a Mie functional form, where the value σ is equivalent to the diameter of the pseudoatoms, the value of the repulsive exponent, n, is fixed, and the parameters ε and m are dependent on both the pseudoatom size and the volume fraction of beads within the spherical shell of the CG nanoparticle. Through parameter optimization for a variety of pseudoatom sizes and volume fractions, functions are

DOI: 10.1021/acs.jctc.8b01269
J. Chem. Theory Comput. 2019, 15, 3260−3271

provided for ϵ and m such that parameters may be obtained for arbitrary nanoparticle models. These parameters are shown to feature transferability across a wide range of nanoparticles sizes, pseudoatom diameters, and volume fractions. It is also shown that a similar approach can be used to obtain cross-interaction parameters between pseudoatoms and other moieties, here specifically CH_2 and CH_3 UA moieties. This allows the model and force field presented herein to have utility toward grafted nanoparticle systems and systems of nanoparticles in solvents. By including long-range target data in the force field optimization, the model presented herein is shown to improve upon prior CG silica nanoparticle models from the literature. This work will help facilitate, among others, studies of nanoparticle self-assembly, with minimal loss of chemical fidelity. The model and optimization scheme is easily extensible to non-silica based nanoparticles as well as silica structures that are non-spherical such as interfaces.

■ ASSOCIATED CONTENT

Supporting Information

The Supporting Information is available free of charge on the ACS Publications website at DOI: 10.1021/acs.jctc.8b01269.

Additional details on the CG nanoparticle model and collection of all-atom target data are provided, along with Python scripts for nanoparticle construction (PDF)

■ AUTHOR INFORMATION

Corresponding Author

*E-mail: c.mccabe@vanderbilt.edu.

ORCID

Andrew Z. Summers: 0000-0001-8477-3059

Clare McCabe: 0000-0002-8552-9135

Funding

Funding for this work has been provided by the National Science Foundation (NSF) through grant ACI-1047827.

Notes

The authors declare no competing financial interest.

■ ACKNOWLEDGMENTS

The authors would like to acknowledge the National Science Foundation (NSF) for providing funding for this work through grant ACI-1047827. A portion of the computational resources for this work were provided by the National Energy Research Scientific Computing Center (NERSC), which is a DOE Office of Science User Facility supported by the Office of Science of the U.S. Department of Energy under contract DE-AC02-05CH11231.

■ REFERENCES

(1) Shim, J.-H.; Lee, B.-J.; Cho, Y. W. Thermal Stability of Unsupported Gold Nanoparticle: A Molecular Dynamics Study. *Surf. Sci.* **2002**, *512* (3), 262−268.

(2) Peters, B. L.; Lane, J. M. D.; Ismail, A. E.; Grest, G. S. Fully Atomistic Simulations of the Response of Silica Nanoparticle Coatings to Alkane Solvents. *Langmuir* **2012**, *28* (50), 17443−17449.

(3) Hong, D.-J.; Lee, E.; Jeong, H.; Lee, J.; Zin, W.-C.; Nguyen, T. D.; Glotzer, S. C.; Lee, M. Solid-State Scrolls from Hierarchical Self-Assembly of T-Shaped Rod-Coil Molecules. *Angew. Chem.* **2009**, *121* (9), 1692−1696.

(4) Van Lehn, R. C.; Alexander-Katz, A. Structure of Mixed-Monolayer-Protected Nanoparticles in Aqueous Salt Solution from Atomistic Molecular Dynamics Simulations. *J. Phys. Chem. C* **2013**, *117* (39), 20104−20115.

(5) Jenkins, S.; Kirk, S. R.; Persson, M.; Carlen, J.; Abbas, Z. Molecular Dynamics Simulation of Nanocolloidal Amorphous Silica Particles: Part I. *J. Chem. Phys.* **2007**, *127* (22), 224711.

(6) Jenkins, S.; Kirk, S. R.; Persson, M.; Carlen, J.; Abbas, Z. Molecular Dynamics Simulation of Nanocolloidal Amorphous Silica Particles: Part II. *J. Chem. Phys.* **2008**, *128* (16), 164711.

(7) Jenkins, S.; Kirk, S. R.; Persson, M.; Carlen, J.; Abbas, Z. Molecular Dynamics Simulation of Nanocolloidal Amorphous Silica Particles: Part III. *J. Chem. Phys.* **2009**, *130* (13), 134702.

(8) Koparde, V. N.; Cummings, P. T. Molecular Dynamics Simulation of Titanium Dioxide Nanoparticle Sintering. *J. Phys. Chem. B* **2005**, *109* (51), 24280−24287.

(9) Xia, Y.; Nguyen, T. D.; Yang, M.; Lee, B.; Santos, A.; Podsiadlo, P.; Tang, Z.; Glotzer, S. C.; Kotov, N. A. Self-Assembly of Self-Limiting Monodisperse Supraparticles from Polydisperse Nanoparticles. *Nat. Nanotechnol.* **2011**, *6* (9), 580−587.

(10) Zhang; Tang; Kotov, N. A.; Glotzer, S. C. Simulations and Analysis of Self-Assembly of CdTe Nanoparticles into Wires and Sheets. *Nano Lett.* **2007**, *7* (6), 1670−1675.

(11) Hattemer, G. D.; Arya, G. Viscoelastic Properties of Polymer-Grafted Nanoparticle Composites from Molecular Dynamics Simulations. *Macromolecules* **2015**, *48* (4), 1240−1255.

(12) Meng, D.; Kumar, S. K.; Lane, J. M. D.; Grest, G. S. Effective Interactions between Grafted Nanoparticles in a Polymer Matrix. *Soft Matter* **2012**, *8* (18), 5002.

(13) Ethier, J. G.; Hall, L. M. Modeling Individual and Pairs of Adsorbed Polymer-Grafted Nanoparticles: Structure and Entanglements. *Soft Matter* **2018**, *14* (4), 643−652.

(14) Chevigny, C.; Dalmas, F.; Di Cola, E.; Gigmes, D.; Bertin, D.; Boué, F.; Jestin, J. Polymer-Grafted-Nanoparticles Nanocomposites: Dispersion, Grafted Chain Conformation, and Rheological Behavior. *Macromolecules* **2011**, *44* (1), 122−133.

(15) Chenoweth, K.; Van Duin, A. C. T.; Goddard, W. A. ReaxFF Reactive Force Field for Molecular Dynamics Simulations of Hydrocarbon Oxidation. *J. Phys. Chem. A* **2008**, *112* (5), 1040−1053.

(16) Pryamtisyn, V.; Ganesan, V.; Panagiotopoulos, A. Z.; Liu, H.; Kumar, S. K. Modeling the Anisotropic Self-Assembly of Spherical Polymer-Grafted Nanoparticles. *J. Chem. Phys.* **2009**, *131* (22), 221102.

(17) Ndoro, T. V. M.; Voyiatzis, E.; Ghanbari, A.; Theodorou, D. N.; Böhm, M. C.; Müller-Plathe, F. Interface of Grafted and Ungrafted Silica Nanoparticles with a Polystyrene Matrix: Atomistic Molecular Dynamics Simulations. *Macromolecules* **2011**, *44* (7), 2316−2327.

(18) Goyal, S.; Escobedo, F. A. Structure and Transport Properties of Polymer Grafted Nanoparticles. *J. Chem. Phys.* **2011**, *135* (18), 184902.

(19) Glotzer, S. C.; Horsch, M. a; Iacovella, C. R.; Zhang, Z.; Chan, E. R.; Zhang, X. Self-Assembly of Anisotropic Tethered Nanoparticle Shape Amphiphiles. *Curr. Opin. Colloid Interface Sci.* **2005**, *10* (5−6), 287−295.

(20) Lamm, M. H.; Chen, T.; Glotzer, S. C. Simulated Assembly of Nanostructured Organic/Inorganic Networks. *Nano Lett.* **2003**, *3* (8), 989−994.

(21) Kumar, S. K.; Krishnamoorti, R. Nanocomposites: Structure, Phase Behavior, and Properties. *Annu. Rev. Chem. Biomol. Eng.* **2010**, *1* (1), 37−58.

(22) Akcora, P.; Liu, H.; Kumar, S. K.; Moll, J.; Li, Y.; Benicewicz, B. C.; Schadler, L. S.; Acehan, D.; Panagiotopoulos, A. Z.; Pryamitsyn, V.; et al. Anisotropic Self-Assembly of Spherical Polymer-Grafted Nanoparticles. *Nat. Mater.* **2009**, *8* (4), 354−359.

(23) Kumar, S. K.; Jouault, N.; Benicewicz, B.; Neely, T. Nanocomposites with Polymer Grafted Nanoparticles. *Macromolecules* **2013**, *46* (9), 3199−3214.

(24) Lane, J. M. D.; Ismail, A. E.; Chandross, M.; Lorenz, C. D.; Grest, G. S. Forces between Functionalized Silica Nanoparticles in Solution. *Phys. Rev. E* **2009**, *79* (5), No. 050501.

(25) Phillips, C. L.; Iacovella, C. R.; Glotzer, S. C. Stability of the Double Gyroid Phase to Nanoparticle Polydispersity in Polymer-Tethered Nanosphere Systems. *Soft Matter* **2010**, *6* (8), 1693.
(26) Liu, J.; Gao, Y.; Cao, D.; Zhang, L.; Guo, Z. Nanoparticle Dispersion and Aggregation in Polymer Nanocomposites: Insights from Molecular Dynamics Simulation. *Langmuir* **2011**, *27* (12), 7926−7933.
(27) Ndoro, T. V. M.; Voyiatzis, E.; Ghanbari, A.; Theodorou, D. N.; Böhm, M. C.; Müller-Plathe, F. Interface of Grafted and Ungrafted Silica Nanoparticles with a Polystyrene Matrix: Atomistic Molecular Dynamics Simulations. *Macromolecules* **2011**, *44* (7), 2316−2327.
(28) Jayaraman, A. Polymer Grafted Nanoparticles: Effect of Chemical and Physical Heterogeneity in Polymer Grafts on Particle Assembly and Dispersion. *J. Polym. Sci., Part B: Polym. Phys.* **2013**, *51* (7), 524−534.
(29) Lafitte, T.; Kumar, S. K.; Panagiotopoulos, A. Z. Self-Assembly of Polymer-Grafted Nanoparticles in Thin Films. *Soft Matter* **2014**, *10* (5), 786−794.
(30) Haley, J. D.; Iacovella, C. R.; Cummings, P. T.; McCabe, C. Examining the Aggregation Behavior of Polymer Grafted Nanoparticles Using Molecular Simulation and Theory. *J. Chem. Phys.* **2015**, *143* (5), No. 054904.
(31) Striolo, A.; McCabe, C.; Cummings, P. T.; Chan, E. R.; Glotzer, S. C. Aggregation of POSS Monomers in Liquid Hexane: A Molecular-Simulation Study. *J. Phys. Chem. B* **2007**, *111* (42), 12248−12256.
(32) Song, X.; Sun, Y.; Wu, X.; Zeng, F. Molecular Dynamics Simulation of a Novel Kind of Polymer Composite Incorporated with Polyhedral Oligomeric Silsesquioxane (POSS). *Comput. Mater. Sci.* **2011**, *50* (12), 3282−3289.
(33) Ionescu, T. C.; Qi, F.; McCabe, C.; Striolo, A.; Kieffer, J.; Cummings, P. T. Evaluation of Force Fields for Molecular Simulation of Polyhedral Oligomeric Silsesquioxanes. *J. Phys. Chem. B* **2006**, *110* (6), 2502−2510.
(34) Klein, C.; Sallai, J.; Jones, T. J.; Iacovella, C. R.; McCabe, C.; Cummings, P. T. A Hierarchical, Component Based Approach to Screening Properties of Soft Matter. In *Foundations of Molecular Modeling and Simulation*; Springer Science + Business Media: Singapore, 2016; pp 79−92.
(35) Iacovella, C. R.; Horsch, M. a; Glotzer, S. C. Local Ordering of Polymer-Tethered Nanospheres and Nanorods and the Stabilization of the Double Gyroid Phase. *J. Chem. Phys.* **2008**, *129* (4), 044902.
(36) Zhang; Horsch, M. A.; Lamm, M. H.; Glotzer, S. C. Tethered Nano Building Blocks: Toward a Conceptual Framework for Nanoparticle Self-Assembly. *Nano Lett.* **2003**, *3* (10), 1341−1346.
(37) Chan, E. R.; Zhang, X.; Lee, C. Y.; Neurock, M.; Glotzer, S. C. Simulations of Tetra-Tethered Organic/Inorganic Nanocube-Polymer Assemblies. *Macromolecules* **2005**, *38* (14), 6168−6180.
(38) In' t Veld, P. J.; Horsch, M. a; Lechman, J. B.; Grest, G. S. Liquid-Vapor Coexistence for Nanoparticles of Various Size. *J. Chem. Phys.* **2008**, *129* (16), 164504.
(39) Girifalco, L. A.; Hodak, M.; Lee, R. S. Carbon Nanotubes, Buckyballs, Ropes, and a Universal Graphitic Potential. *Phys. Rev. B: Condens. Matter Mater. Phys.* **2000**, *62* (19), 13104−13110.
(40) Izvekov, S.; Violi, A.; Voth, G. a. Systematic Coarse-Graining of Nanoparticle Interactions in Molecular Dynamics Simulation. *J. Phys. Chem. B* **2005**, *109* (36), 17019−17024.
(41) Chan, E. R.; Striolo, A.; McCabe, C.; Cummings, P. T.; Glotzer, S. C. Coarse-Grained Force Field for Simulating Polymer-Tethered Silsesquioxane Self-Assembly in Solution. *J. Chem. Phys.* **2007**, *127* (11), 114102.
(42) Moore, T. C.; Iacovella, C. R.; McCabe, C. Derivation of Coarse-Grained Potentials via Multistate Iterative Boltzmann Inversion. *J. Chem. Phys.* **2014**, *140* (22), 224104.
(43) Lee, C. K.; Hua, C. C. Nanoparticle Interaction Potentials Constructed by Multiscale Computation. *J. Chem. Phys.* **2010**, *132* (22), 224904.
(44) Toth, G. Effective Potentials from Complex Simulations: A Potential-Matching Algorithm and Remarks on Coarse-Grained Potentials. *J. Phys.: Condens. Matter* **2007**, *19* (33), 335222.
(45) Summers, A. Z.; Iacovella, C. R.; Cane, O. M.; Cummings, P. T.; McCabe, C. *NanoOpt: Deriving potentials for coarse-grained nanoparticles via potential-matching*. https://github.com/mosdef-hub/nanoparticle_optimization (accessed December 8, 2018).
(46) *MoSDeF Github*. https://github.com/mosdef-hub (accessed July 10, 2017).
(47) Ramrattan, N. S.; Avendaño, C.; Müller, E. A.; Galindo, A. A Corresponding-States Framework for the Description of the Mie Family of Intermolecular Potentials. *Mol. Phys.* **2015**, *113* (9−10), 932−947.
(48) Litton, D. A.; Garofalini, S. H. Modeling of Hydrophilic Wafer Bonding by Molecular Dynamics Simulations. *J. Appl. Phys.* **2001**, *89* (11), 6013−6023.
(49) Fogarty, J. C.; Aktulga, H. M.; Grama, A. Y.; van Duin, A. C. T.; Pandit, S. A. A Reactive Molecular Dynamics Simulation of the Silica-Water Interface. *J. Chem. Phys.* **2010**, *132* (17), 174704.
(50) Black, J. E.; Iacovella, C. R.; Cummings, P. T.; McCabe, C. Molecular Dynamics Study of Alkylsilane Monolayers on Realistic Amorphous Silica Surfaces. *Langmuir* **2015**, *31* (10), 3086−3093.
(51) Summers, A. Z.; Iacovella, C. R.; Cummings, P. T.; McCabe, C. Investigating Alkylsilane Monolayer Tribology at a Single-Asperity Contact with Molecular Dynamics Simulation. *Langmuir* **2017**, *33* (42), 11270−11280.
(52) Aktulga, H. M.; Fogarty, J. C.; Pandit, S. a.; Grama, a. Y. Parallel Reactive Molecular Dynamics: Numerical Methods and Algorithmic Techniques. *Parallel Comput.* **2012**, *38* (4−5), 245−259.
(53) Nosé, S. A Unified Formulation of the Constant Temperature Molecular Dynamics Methods. *J. Chem. Phys.* **1984**, *81* (1), 511.
(54) Hoover, W. G. Canonical Dynamics: Equilibrium Phase-Space Distributions. *Phys. Rev. A: At., Mol., Opt. Phys.* **1985**, *31* (3), 1695−1697.
(55) Plimpton, S. Fast Parallel Algorithms for Short-Range Molecular Dynamics. *J. Comput. Phys.* **1995**, *117* (1), 1−19.
(56) *LAMMPS web page*. http://lammps.sandia.gov (accessed 11-15-2018).
(57) Sun, H. Ab Initio Calculations and Force Field Development for Computer Simulation of Polysilanes. *Macromolecules* **1995**, *28* (3), 701−712.
(58) Sun, H.; Rigby, D. Polysiloxanes: Ab Initio Force Field and Structural, Conformational and Thermophysical Properties. *Spectrochim. Acta, Part A* **1997**, *53* (8), 1301−1323.
(59) Ionescu, T. C.; Qi, F.; McCabe, C.; Striolo, A.; Kieffer, J.; Cummings, P. T. Evaluation of Force Fields for Molecular Simulation of Polyhedral Oligomeric Silsesquioxanes. *J. Phys. Chem. B* **2006**, *110* (6), 2502−2510.
(60) Waldman, M.; Hagler, A. T. New Combining Rules for Rare Gas van Der Waals Parameters. *J. Comput. Chem.* **1993**, *14* (9), 1077−1084.
(61) Frischknecht, A. L.; Curro, J. G. Improved United Atom Force Field for Poly(Dimethylsiloxane). *Macromolecules* **2003**, *36* (6), 2122−2129.
(62) Anderson, J. A.; Lorenz, C. D.; Travesset, A. General Purpose Molecular Dynamics Simulations Fully Implemented on Graphics Processing Units. *J. Comput. Phys.* **2008**, *227* (10), 5342−5359.
(63) Glaser, J.; Nguyen, T. D.; Anderson, J. A.; Lui, P.; Spiga, F.; Millan, J. A.; Morse, D. C.; Glotzer, S. C. Strong Scaling of General-Purpose Molecular Dynamics Simulations on GPUs. *Comput. Phys. Commun.* **2015**, *192*, 97−107.
(64) Jones, E.; Oliphant, T. E.; Peterson, P.; Al, E. *SciPy: Open source scientific tools for Python*. http://www.scipy.org/ (accessed July 11, 2018).
(65) Nelder, J. A.; Mead, R. A Simplex Method for Function Minimization. *Comput. J.* **1965**, *7* (4), 308−313.
(66) Wright, M. H. Direct Search Methods: Once Scorned, Now Respectable. In *Numerical Analysis*; Griffiths, D. F., Watson, G. A., Eds.; Addison Wesley Longman: Harlow, UK, 1996; pp 191−208.

DOI: 10.1021/acs.jctc.8b01269
J. Chem. Theory Comput. 2019, 15, 3260−3271

(67) Nielsen, S. O.; Lopez, C. F.; Srinivas, G.; Klein, M. L. A Coarse Grain Model for N-Alkanes Parameterized from Surface Tension Data. *J. Chem. Phys.* **2003**, *119* (14), 7043.
(68) Moore, T. C.; Iacovella, C. R.; Hartkamp, R.; Bunge, A. L.; McCabe, C. A Coarse-Grained Model of Stratum Corneum Lipids: Free Fatty Acids and Ceramide NS. *J. Phys. Chem. B* **2016**, *120* (37), 9944−9958.
(69) Marrink, S. J.; Mark, A. E. The Mechanism of Vesicle Fusion as Revealed by Molecular Dynamics Simulations. *J. Am. Chem. Soc.* **2003**, *125* (37), 11144−11145.
(70) Arnarez, C.; Uusitalo, J. J.; Masman, M. F.; Ingólfsson, H. I.; De Jong, D. H.; Melo, M. N.; Periole, X.; De Vries, A. H.; Marrink, S. J. Dry Martini, a Coarse-Grained Force Field for Lipid Membrane Simulations with Implicit Solvent. *J. Chem. Theory Comput.* **2015**, *11* (1), 260−275.
(71) Martin, M. G.; Siepmann, J. I. Transferable Potentials for Phase Equilibria. 1. United-Atom Description of *n*-Alkanes. *J. Phys. Chem. B* **1998**, *102*, 2569.

DOI: 10.1021/acs.jctc.8b01269
J. Chem. Theory Comput. 2019, 15, 3260−3271